catalysts

MDPI

Article

Construction of Palladium Nanoparticles Modified Covalent Triazine Frameworks towards Highly-Efficient Dehydrogenation of Dipentene for p-Cymene Production

Yanni Liu [1], Yonghui Chen [2], Yikai Wang [2], Zijie Xiao [2], Yilin Chen [2], Jianchun Jiang [3,4], Xiaoping Rao [1,*] and Yun Zheng [2,*]

[1] Academy of Advanced Carbon Conversion Technology, Huaqiao University, Xiamen 361021, China; 22014087018@stu.hqu.edu.cn
[2] Xiamen Key Laboratory of Optoelectronic Materials and Advanced Manufacturing, College of Materials Science and Engineering, Huaqiao University, Xiamen 361021, China; chen18755289963@163.com (Y.C.); loyce@stu.hqu.edu.cn (Y.W.); 21013081030@stu.hqu.edu.cn (Z.X.); ylchen@hqu.edu.cn (Y.C.)
[3] Institute of Chemical Industry of Forest Products, Chinese Academy of Forestry (CAF), No. 16, Suojin Five Village, Nanjing 210042, China; jiangjc@icifp.cn
[4] Jiangsu Co-Innovation Center for Efficient Processing and Utilization of Forest Resources, College of Chemical Engineering, Nanjing Forestry University, Longpan Road 159, Nanjing 210037, China
* Correspondence: raoxp@hqu.edu.cn (X.R.); zheng-yun@hqu.edu.cn (Y.Z.)

Abstract: The generation of p-cymene from the catalytic dehydrogenation of dipentene is one of the most vital approaches for the synthesis of p-cymene in the chemical industry. Herein, CTF polymer was synthesized by an ionothermal method via using terephthalonitrile as monomer and NaCl-KCl-$ZnCl_2$ ternary mixture as catalyst and solvent, and Pd/CTF catalyst was prepared by loading CTF matrix with Pd nanoparticles via a chemical reduction method. The as-obtained Pd/CTF catalyst with the loading amount of 5 wt% Pd showed remarkable catalytic activity in the dehydrogenation of dipentene to p-cymene with a high conversion rate of 100% and a high selectivity of 96% at the reaction temperature of 220 °C in a stainless-steel autoclave containing 0.1 MPa of Ar gas, and also exhibited good stability in the recycling tests. The strong interaction between Pd nanoparticles and CTF and the enhanced electron transfer at the metal-semiconductor interface contribute to the outstanding catalytic performance of Pd/CTF for the dehydrogenation of dipentene to p-cymene. This work demonstrates that the metal-semiconductor catalysts possessed excellent potential in the production of high-value-added chemical products from terpenes conversion.

Keywords: palladium nanoparticles; covalent triazine frameworks; catalysis; dehydrogenation; dipentene

check for updates

Citation: Liu, Y.; Chen, Y.; Wang, Y.; Xiao, Z.; Chen, Y.; Jiang, J.; Rao, X.; Zheng, Y. Construction of Palladium Nanoparticles Modified Covalent Triazine Frameworks towards Highly-Efficient Dehydrogenation of Dipentene for p-Cymene Production. *Catalysts* **2023**, *13*, 1248. https://doi.org/10.3390/catal13091248

Academic Editors: Bo Weng, Xiaoyang Pan and Bin Han

Received: 30 July 2023
Revised: 20 August 2023
Accepted: 26 August 2023
Published: 28 August 2023

Copyright: © 2023 by the authors. Licensee MDPI, Basel, Switzerland. This article is an open access article distributed under the terms and conditions of the Creative Commons Attribution (CC BY) license (https://creativecommons.org/licenses/by/4.0/).

1. Introduction

The catalytic conversion of renewable biomass terpenes into value-added chemicals has long been a research area of considerable importance for sustainable development [1–3]. Industrial dipentene is mainly composed of various monoterpenes, including isomers of limonene, terpinenes, terpinolene, and other menthadienes [4]. As a by-product of the pulp-paper industry and camphor preparation with very low price, industrial dipentene could serve a natural, renewable, abundantly available, and low-cost feedstock for p-cymene synthesis due to its vast production [5].

Due to its similar molecular structure, p-cymene is the most promising and valuable product obtained from industrial dipentene dehydrogenation [6,7]. p-cymene is one of the most important and valuable ingredients in flavorings and fragrances [8]. p-cymene can be converted into p-cresol or 4-isopropylbenzaldehyde in different oxidation conditions [9]. Additionally, p-cymene serves as a solvent for organic transformation, a heat transfer medium, and an odor masking agent for industrial products [10–12].

Traditionally, p-cymene is produced from petroleum feedstocks through Friedel–Crafts alkylation of toluene with propylene or 2-propanol [13]. Nevertheless, to achieve good catalytic performance in this reaction, hazardous acids such as $AlCl_3$ or HF must be used, leading to problems with safety, corrosion, waste disposal, and environmental pollution. An alternative method to produce p-cymene from the dehydrogenation of terpenes (Figure 1) showed tremendous benefits of high activity, shape selectivity, and an eco-friendly approach [14–19]. In recent decades, a variety of heterogeneous catalysts have been prepared and applied to the dehydrogenation reaction of terpene to p-cymene in the liquid or gas phase [20]. These catalysts include Ti/SBA-15 (liquid phase, 160 °C, 56% p-cymene yield) [21], Pd/HZSM-5 (liquid phase, 260 °C, 8 bar, 82% yield) [22], Pd/Al_2O_3 (supercritical ethanol, 300 °C, 65 bar, 80% yield) [23], Zn/SBA-15 (gas phase, 450 °C, 86.7% p-cymene yield) [24], TiO_2 (gas phase, 300 °C, 90% yield) [25], Pd/SiO_2 (gas phase, 300 °C, in H_2 flow, 99% yield) [26], ZnO/SiO_2 (gas phase, 370 °C, 90% yield) [27], and CdO/SiO_2 (gas phase, 200–250 °C, 91–100% yield) [28]. When zeolites and alkali metals are used as catalysts for liquid-phase dehydrogenation, the reaction conditions for liquid phase dehydrogenation are milder, but the yield of p-cymene is not ideal. When metal oxides are used as catalysts for gas-phase dehydrogenation, a high conversion rate of dipentene are achieved. However, the problem of gas-phase dehydrogenation is higher reaction temperature, more requirements for equipment, and higher production costs. Therefore, the development of highly efficient catalysts is vital for realizing the high-yield production of p-cymene from dehydrogenation of terpene at mild conditions.

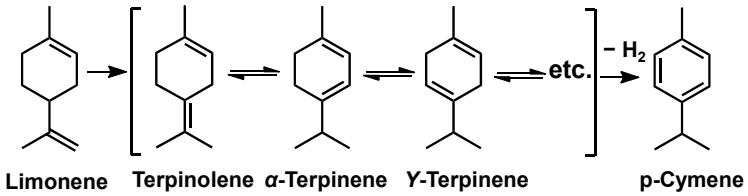


Figure 1. Reaction pathway for the dehydroisomerization of limonene to p-cymene.

Noble metal catalysts, such as palladium, platinum, etc., showed high catalytic activity for the dehydrogenation of aromatic compounds at mild conditions [29]. It is expected to raise the yield of p-cymene, increase the stability and recyclability of the catalyst, and make the reaction conditions more moderate by selecting suitable support to deposit noble metals. Covalent triazine framework (CTF) is a kind of covalent organic framework material that has the characteristics of nitrogen-rich, organic conjugated structure and good stability, and is a promising catalyst support in heterogeneous catalysis [30–32]. CTF is composed of aromatic N-C=N structure of triazine ring unit by covalent bond. However, most CTF materials have the problem of high exciton binding energy and weak electron transport capacity [33,34]. Nitrogen in CTF can improve the catalytic reaction performance of supported palladium nanoparticles in the following aspects: (1) The nitrogen sites (particularly sp^2 N-C=N nitrogen in the triazine unit) can provide anchoring sites for metals, so that the metal nanoparticles can be evenly dispersed and anchored on the support, and the size of the metal nanoparticles can be finely controlled; (2) The negative electrical properties presented by the nitrogen site can increase the electron density of the metal particles so that the metal can maintain a high catalytic performance; (3) nitrogen sites could remain the metal in metallic state during air contact, and metal on nitrogen sites may promote absorption of reactants or desorption of products [35–38]. Therefore, palladium nanoparticles loaded on CTF could serve as a potential candidate for catalyzing dehydrogenation of dipentene to p-cymene with good catalytic performance and high stability.

Herein, CTF polymer was synthesized by an ionothermal method via using terephthalonitrile as monomer and NaCl-KCl-$ZnCl_2$ ternary mixture as catalyst and solvent. A series of Pd/CTF catalysts with various Pd loading amounts were prepared by a chemical reduction method and further applied to catalyze the dehydrogenation of dipentene to pre-

pare p-cymene. The effect of different Pd loading amounts on the composition, morphology, and catalytic activity of Pd/CTF catalysts were analyzed. This work has significance for the development of catalysts and high-value utilization of biomass that meet the demand of green chemistry and sustainable development.

2. Results and Discussion

A scanning electron microscope (SEM) and transmission electron microscope (TEM) were employed to reveal the morphology of Pd/CTF catalysts. As shown in the SEM images, 5% Pd/CTF catalyst presents the morphology of stacked layered structure (Figure 2a). The TEM image of 5% Pd/CTF displayed that Pd nanoparticles are uniformly dispersed on the nanosheets of CTF (Figure 2b). The dark-field high angle annular dark field-scanning transmission electron microscopy) (HAADF-STEM) image and TEM elemental mapping image of 5% Pd/CTF verified that C, N, and Pd elements are evenly distributed in the 5% Pd/CTF sample, indicating that Pd nanoparticles are uniformly dispersed on CTF nanosheets (Figure 2c–f). The energy dispersive spectrum (EDS) of 5% Pd/CTF in Figure 2g demonstrated that 5% Pd/CTF is mainly composed of C, N, and Pd elements. The high-resolution transmission electron microscope (HR-TEM) image of 5% Pd/CTF displayed distinct lattice fringes with a lattice spacing of 0.224 nm for Pd nanoparticles, corresponding to the Pd (111) crystal planes (Figure 2h).

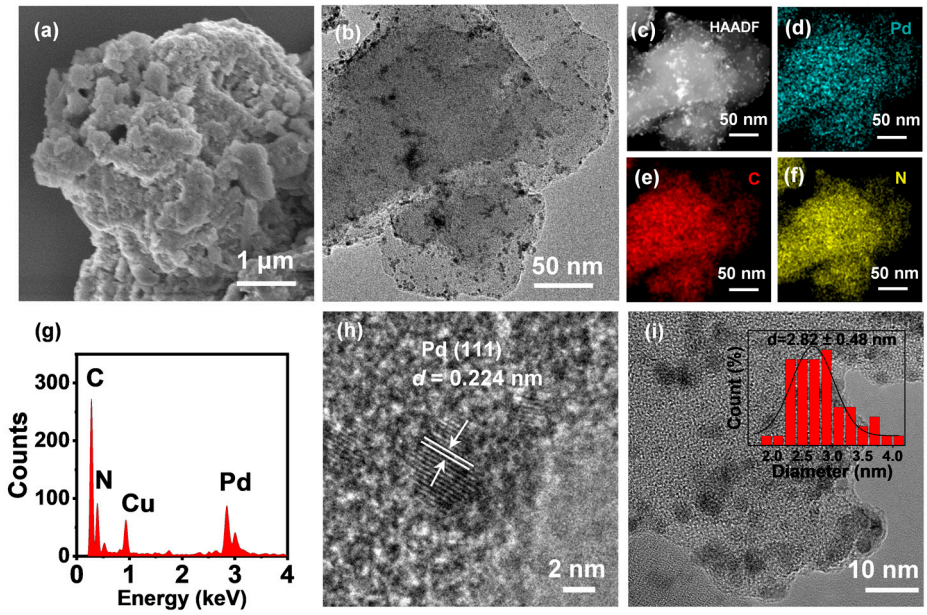


Figure 2. (**a**) SEM image, (**b**) TEM image, (**c**) dark-field HAADF-STEM image, TEM elemental mapping images of (**d**) Pd, (**e**) C, and (**f**) N. (**g**) TEM-EDS spectra, (**h**) HR-TEM image of 5% Pd/CTF showing Pd (111) crystal planes, and (**i**) TEM image of 5% Pd/CTF and size distribution of Pd nanoparticles on CTF (inset).

The particle size distributions of Pd nanoparticles were investigated based on the TEM images of Pd/CTF catalysts with different Pd loading amounts. The statistical analysis of the particle size results is shown in Figure S1 and Table S1. Among the Pd/CTF catalysts with different Pd loading amounts, 5% Pd/CTF catalysts possessed the smallest sizes of Pd nanoparticles (2.82 ± 0.48 nm, Figure 2i). The presence of nitrogen groups in CTF has a positive effect on the uniform dispersion of small-sized Pd nanoparticles. The better dispersion of Pd nanoparticles is one of the major reasons for the high catalytic activity of Pd/CTF. Additionally, a larger average diameter and a wider diameter distribution of Pd nanoparticles on activated carbon (AC) than those of CTF were observed. The wilder diameter distribution of Pd nanoparticles on AC could be attributed to the irregular porous structure of AC and random anchoring sites.

X-ray powder diffraction (XRD) and Fourier transform infrared (FT-IR) spectra were recorded to probe the composition and chemical structure of Pd/CTF catalysts. The XRD patterns of Pd/CTF and CTF are shown in Figure 3a. Both CTF and Pd/CTF samples showed the diffraction peaks at 7.6°, 14.4°, 15.4° and 26.6°, correspond to $\{10\bar{1}0\}$, $\{11\bar{2}0\}$, $\{20\bar{2}0\}$, and {0002} crystal planes, respectively. The two broad characteristic peaks at 14.4° and 26.6° correspond to the long-range in-plane molecular ordering of triazine-based polymers and the interlayer packing of π-conjugated aromatic structures, respectively [39–42]. The major structure of CTF is still retained after Pd loading treatment. In comparison with pristine CTF, the XRD patterns of Pd/CTF sample also presented the peaks at 39.8°, 46.0°, and 68.1°, corresponding to the (111), (200), and (220) planes of cubic Pd (JCPDS No. 88-2335), respectively. In addition, no obvious diffraction peaks of KCl, LiCl, and $ZnCl_2$ were observed for both CTF and Pd/CTF catalysts, suggesting that KCl, LiCl, and $ZnCl_2$ have been completely removed after the washing process.

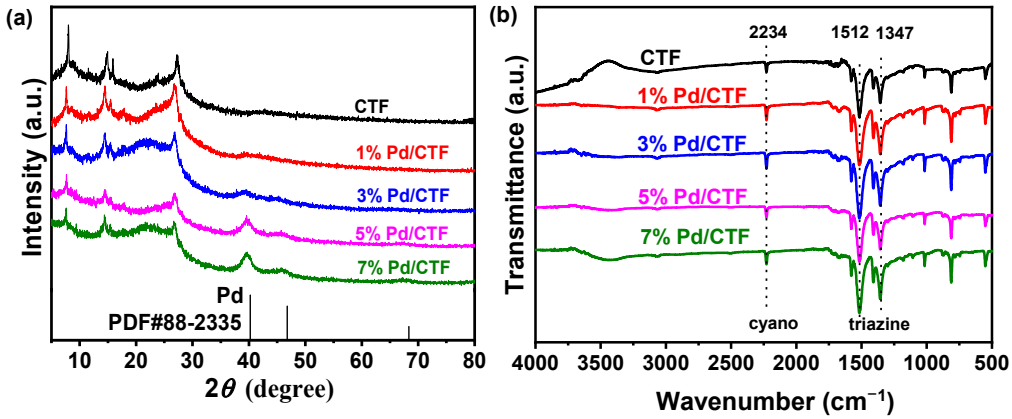


Figure 3. (**a**) XRD patterns, and (**b**) FT-IR spectra of CTF and Pd/CTF.

The Fourier transform infrared (FT-IR) spectra of Pd/CTF is shown in Figure 3b. The absorption bands in the range of 800–1800 cm^{-1} are the characteristic absorption of the benzene ring and triazine ring. The stretching mode of C-N bond of the triazine ring at 1347 cm^{-1} and 1512 cm^{-1} indicates that the aromatic nitrile precursors were successfully polymerized. The peak at 2234 cm^{-1} was attributed to the unreacted cyano group at the end of CTF. The similar FT-IR spectra of Pd/CTF samples and CTF suggested that no significant structural change of CTF occurred after loading with Pd nanoparticles.

The surface composition and electronic structure of CTF and Pd/CTF samples were studied by X-ray photoelectron spectra (XPS) in order to survey the interaction between Pd species and CTF support. It can be seen that the main constituent elements of 5% Pd/CTF sample are Pd, C, N, and O (Figure 4a). The presence of O is due to the presence of water and/or oxygen absorbed from the ambient atmosphere or the spontaneous surface oxidation of Pd nanoparticles. No additional elemental peaks of Na, K, Zn, and Cl were found, indicating that the salts of NaCl, KCl, and $ZnCl_2$ can be removed by washing with water and acid. In the C 1s spectrum, 284.8 eV corresponds to the binding energy of sp^2 hybridized C=C and methylene C-H bonds on the benzene ring, and 286.8 eV corresponds to the binding energy of N-C=N on the triazine ring (Figure 4b).

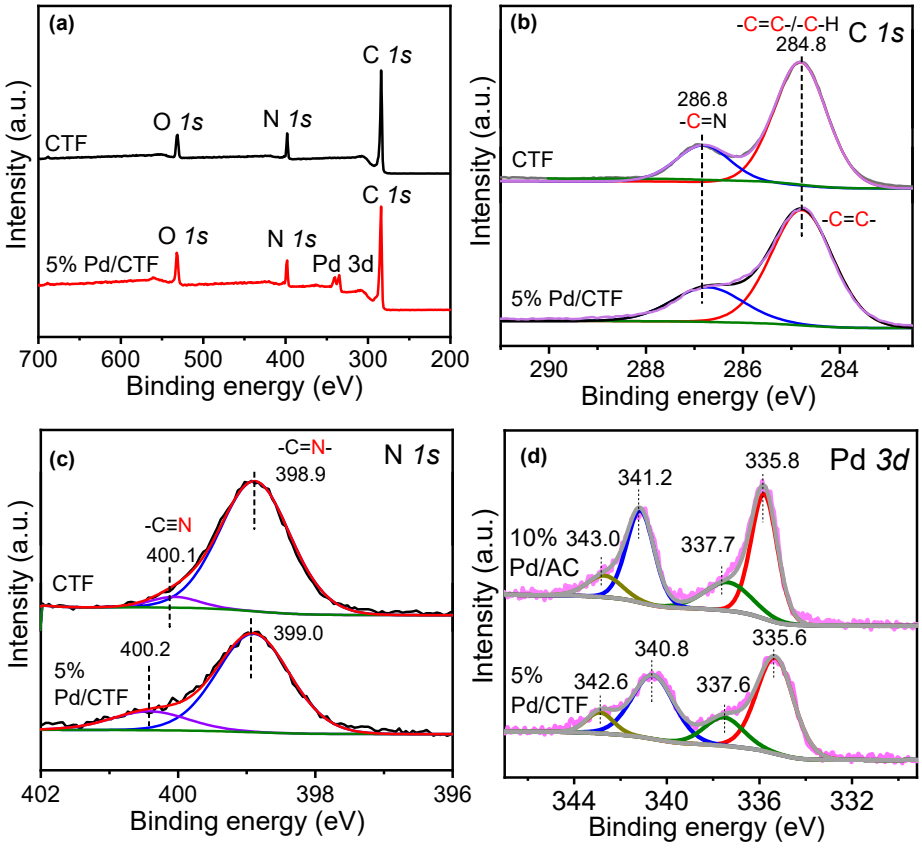


Figure 4. XPS spectra of (**a**) survey, (**b**) C 1s, (**c**) N 1s, and (**d**) Pd 3d for CTF, 5% Pd/CTF and 10% Pd/AC catalyst.

The N 1s spectrum shows that CTF and 5% Pd/CTF contain two groups of peaks at 399.0 eV and 400.1 eV, corresponding to the sp^2 hybrid nitrogen (C-N=C) and the terminal C≡N group on the triazine ring, respectively (Table S2). The structure contains cyano groups, which is consistent with the results of FT-IR spectroscopy. It is noted that the N 1s peak of Pd/CTF gradually shifts towards higher binding energy than that of CTF, suggesting the decreased electron density of nitrogen and the transfer of electrons from CTF to Pd (Figure 4c). Such a shift in XPS verified the electron donation from support to metallic Pd nanoparticles owing to the intensified electronic interactions between the Pd nanoparticles and N in CTF support. This result is consistent with the metal nanoparticles supported on N-doped carbon nanotubes and N-containing species in previous studies [43–47]. Since N atoms in CTF are essentially in sp^2 hybridization, the lone electron pairs of N are effective Lewis bases that affect the electronic structure of Pd attached to them. These π-bonded planar C-N-C structures, along with the unsaturated nitrogen groups in the edges of the CTF support, are suitable sites for anchoring Pd^0 particles, where strong metal-support interaction occurred.

Additionally, the Pd 3d spectra for Pd nanoparticles on CTF can be resolved into two spin-orbit pairs with 3d3/2 binding energies of 342.6 eV and 340.8 eV, and with 3d5/2 binding energies of 337.6 eV and 335.6 eV, respectively (Figure 4d). The peaks at 342.6 eV (Pd 3d3/2) and 337.6 eV (Pd 3d5/2) are attributed to Pd^{2+}, while the peaks at 340.8 eV (Pd 3d3/2) and 335.6 eV (Pd 3d5/2) are attributed to Pd^0. It is noted that the peaks at 340.8 eV (Pd 3d3/2) and 335.6 eV (Pd 3d5/2) attributing to Pd^0 for 5% Pd/CTF show down shift of 0.2–0.4 eV when compared with those of 10% Pd/AC. A similar shift can also be observed from supported catalysts in other reports, confirming the electron transfer between support and catalyst [48–50].

The components of industrial dipentene were analyzed by GC-MS spectra. Table 1 shows that the sum of the mass fractions of four components belonging to the dipentene series in the industrial dipentene raw materials, including α-terpinene, limonene, γ-terpinene,

and terpinene, is 89.38%. It also contains p-cymene (9.72%) and a small amount of carene and camphene.

Table 1. Analysis results of industrial dipentene by GC-MS spectra.

Entry	Retention Time/Min	Content/ %	Molecular Formula	Relative Molecular Mass	Chemical Compound
1	7.345	0.37	$C_{10}H_{16}$	136	Camphene
2	9.263	0.53	$C_{10}H_{16}$	136	3-Carene
3	9.477	9.82	$C_{10}H_{16}$	136	α-Terpinene
4	9.761	9.72	$C_{10}H_{14}$	134	p-Cymene
5	9.921	36.52	$C_{10}H_{16}$	136	D-Limonene
6	11.147	7.45	$C_{10}H_{16}$	136	γ-Terpinene
7	12.402	35.59	$C_{10}H_{16}$	136	Terpinolene

Additionally, the components of the liquid product produced by using 5% Pd/CTF catalyst were investigated by GC-MS spectra. Table 2 is the GC-MS analysis results of industrial dipentene dehydrogenation products. At the temperature of 220 °C, the liquid product of p-cymene in the dehydrogenation reaction of dipentene catalyzed by 5% Pd/CTF mainly contains 95.85% of p-cymene, and contains a small amount (4.15%) of p-menthane.

Table 2. Analysis results of liquid product by GC-MS spectra.

Entry	Retention Time/Min	Content/ %	Molecular Formula	Relative Molecular Mass	Chemical Compound
1	8.117	4.15	$C_{10}H_{20}$	140	p-Menthane
2	9.771	95.85	$C_{10}H_{14}$	134	p-Cymene

The catalytic activity of Pd/CTF in the dehydrogenation of dipentene to p-cymene was investigated. First, the effect of Pd loading amount on the catalytic activity of Pd/CTF was studied. Table 3 shows the conversion rate of dipentene and the selectivity and content to cymene for Pd/CTF with different Pd loading amounts. Among Pd/CTF samples with different Pd loadings, 5% Pd/CTF catalyzed the dehydrogenation of dipentene to prepare p-cymene with the best catalytic effect. The conversion rate of dipentene is close to 100%, and the selectivity to p-cymene reaches 95.85%. However, reducing the Pd loading to 0.5% or increasing to 7% reduced the p-cymene content in the product. The catalytic effect of pristine CTF is poor in the absence of Pd.

Table 3. The conversion rate of dipentene, the selectivity of p-cymene, and the content of p-cymene for Pd/CTF with different Pd contents.

Entry	Catalyst	Reaction Temperature (°C)	Conversion of Dipentene (%)	Selectivity of p-Cymene (%)	Content of p-Cymene (%)
1	5% Pd/CTF	220	100	95.85	95.85
2	0.5% Pd/CTF	220	91.25	66.60	72.99
3	1% Pd/CTF	220	100	85.61	85.61
4	3% Pd/CTF	220	100	86.75	86.75
5	7% Pd/CTF	220	100	86.04	86.04

Second, the catalytic activities of different types of catalysts were compared. It can be seen from Table 4 that the catalytic performance of 5% Pd/CTF is higher than that of unloaded CTF, commercial 10% Pd/AC, H-ZSM-5 molecular sieve (Si/Al = 30), Raney Ni,

commercial Pd/AC, and Raney Ni mixture (mixed at a mass ratio of 1:1). When no catalyst was added and the products was only heated at 220 °C for 6 h, the content of p-cymene in the product was very low (<20%), which indicated that the catalyst played an important role in promoting the dehydrogenation of dipentene.

Table 4. The conversion rate of dipentene, the selectivity of p-cymene, and the content of p-cymene for different kinds of catalysts.

Entry	Catalyst	Reaction Temperature (°C)	Conversion of Dipentene (%)	Selectivity of p-Cymene (%)	Content of p-Cymene (%)
1	5% Pd/CTF	220	100	95.85	95.85
2	10% Pd/AC	220	100	82.26	82.26
3	H-ZSM-5(Si/Al = 30)	220	96.51	58.36	60.47
4	Raney Ni	220	68.63	28.30	41.24
5	10%Pd/AC+ Raney Ni (1:1)	220	85.04	61.08	71.83
6	M-CTF	220	50.31	7.94	15.79

In addition, we performed XPS characterization of Pd/CTF with different loadings, commercial Pd/AC, as well as 5% Pd/CTF after use and commercial Pd/AC after use. The XPS results of the Pd^0/Pd_{total} ratios of Pd/CTF with different palladium loadings, calculated from the peak areas of Pd^0 and Pd^{2+}, are shown in Figure S2 and Table S1. The Pd^0/Pd_{total} increases and then decreases with the increase of the loading amount of Pd/CTF. The Pd^0 ratio of 1% Pd/CTF is lower, which is probably due to the lower surface Pd content and higher surface N content. 5% Pd/CTF has the highest Pd^0/Pd_{total} ratio of 92.20%, which may be due to the uniform dispersion of Pd nanoparticles on the layered CTF. Interestingly, this coincides well with the minimum particle size and the highest catalytic dehydrogenation activity of 5% Pd/CTF, as mentioned earlier. We noted that 7% Pd/CTF shows a decrease in the Pd^0 ratio, which may be due to the oxidation of part of the Pd^0 to Pd^{2+}. However, the active phase in the reaction is Pd^0 [51]. The small amount of Pd^{2+} is due to the oxidation of Pd in air, which is a common phenomenon for Pd-based catalysts [52]. Meanwhile, the CTF support also stabilized Pd^0, which was confirmed in the XPS spectra, and the excellent catalytic performance of Pd/CTF is precisely because the highly dispersed nanoparticles can provide more active sites and interaction force with the support [53].

As shown in Figure S3 and Table S1, the Pd^0 content in 5% Pd/CTF after use still reached 91.5%, which is an important reason why its catalytic activity remained almost unchanged after cyclic reaction. The C 1s and N 1s spectra demonstrated that the major chemical structure of CTF support remained after dehydrogenation reactions of 5%Pd/CTF catalyst (Figure S4). However, Pd^0 content of 10% Pd/AC decreased more rapidly from 87.86% to 80.89% after dehydrogenation reactions. The significantly decreased Pd^0 content is related to the decreased stability and catalytic activity of 10% Pd/AC for dehydrogenation reactions.

Again, the effect of different reaction temperatures on the catalytic activity of 5% Pd/CTF was explored. It can be seen from Table 5 that when the reaction temperature is 160 °C, the conversion rate (96.25%) and selectivity (77.05%) of dipentene dehydrogenation reaction catalyzed by 5% Pd/CTF are low, and the content of p-cymene in the product is only 80.05%. When the reaction temperature increased from 160 °C to 220 °C, the content of p-cymene in the dehydrogenation of dipentene catalyzed by 5% Pd/CTF also increased. This is because the reaction of dipentene dehydrogenation to p-cymene is an endothermic reaction with a relatively significant thermal effect, and increasing the reaction temperature in a suitable temperature range is beneficial to the generation of p-cymene. When the temperature is 220 °C, 5% Pd/CTF has the best catalytic effect. However, when the temperature exceeds 220 °C, for example, when it is set to 240 °C, the content of p-cymene in the catalyzed product of 5% Pd/CTF decreases slightly. Therefore, the present

system prefers 220 °C as the optimal reaction temperature for preparing p-cymene via the dehydrogenation of dipentene.

Table 5. The conversion rate of dipentene, the selectivity of p-cymene, and the content of p-cymene at different reaction temperatures.

Entry	Catalyst	Reaction Temperature (°C)	Conversion of Dipentene (%)	Selectivity of p-Cymene (%)	Yield (%)				
					A	B	C	D	E
1	5% Pd/CTF	220	100	95.85		4.15	95.85		
2	5% Pd/CTF	160	96.25	77.05	4.55	6.59	80.05		5.06
3	5% Pd/CTF	180	97.75	80.57	4.87	6.90	82.42		3.56
4	5% Pd/CTF	200	100	83.14	5.58	7.58	83.14		3.70
5	5% Pd/CTF	240	100	88.16		11.84	88.16		

The possible products (as shown in Figure 5) mainly include A: Partial hydrogenation products (Carvomenthene and β-Dihydrolimonene); B: Full hydrogenation products (p-menthane); C: Dehydroaromatization products (p-cymene); D: Isomerization products (terpinolene, α-terpinolene, γ-terpinolene, α-phellandrene); E: Light (Other organic products without a ring structure). The yields of these products are shown in Table 5. At a low reaction temperature, the dehydrogenation reaction and hydrogenation reaction proceed at the same time, in which the hydrogen produced and the intermediate generated a partially hydrogenated product and a completely hydrogenated product, respectively. As reaction temperature increased, the rapid progress of the dehydrogenation reaction and the formation of a stable aromatisation product occurred, and it is difficult to form a hydrogenated product. The side reaction is suppressed in disguise. However, when the temperature is too high, the rate of dehydrogenation reaction and hydrogenation reaction is accelerated at the same time, resulting in a low reaction effect. Therefore, it is considered here that the difference in the rates of dehydrogenation and hydrogenation reactions is influenced by the change in the reaction process and reaction temperature.

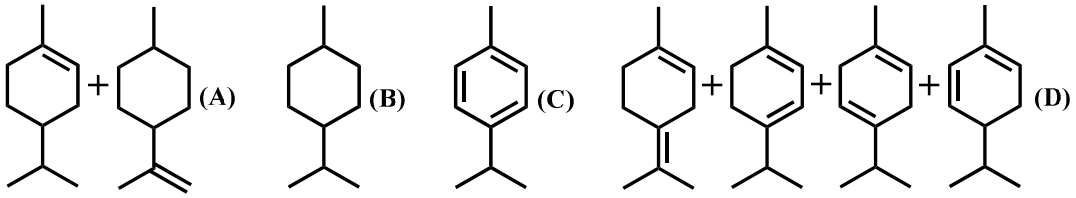


Figure 5. Chemical structures of the possible products from dipentene dehydrogenation.

General conditions: 0.1 g of catalyst, 5 g of industrial dipentene, 220 °C, 0.1 MPa Ar gas, 240 min, stirring at 300 rpm.

Finally, the stability of Pd/CTF catalyst was investigated. It can be seen from Table 6 that the 5% Pd/CTF sample after the reaction was recovered and reused four times. A very slight decreasing catalytic activity was observed after four times of testing for 5% Pd/CTF. However, when the commercial palladium carbon (10% Pd/AC) is reused four times, the reduction in the content of p-cymene in the product is more obvious (Table 7). Thus, Pd/CTF exhibited higher stability than Pd/AC in the dehydrogenation of dipentene.

Table 6. The conversion rate of dipentene, the selectivity of p-cymene, and the content of p-cymene for repeated use of Pd/CTF.

Entry	Catalyst	Reaction Temperature (°C)	Conversion of Dipentene (%)	Selectivity of p-Cymene (%)	Content of p-Cymene (%)
1	5% Pd/CTF (First run)	220	100	95.85	95.85
2	5% Pd/CTF (Second run)	220	100	95.54	95.54
3	5% Pd/CTF (Third run)	220	100	95.02	95.02
4	5% Pd/CTF (Forth run)	220	100	94.58	94.58

Table 7. The conversion rate of dipentene, the selectivity of p-cymene, and the content of p-cymene for repeated use of Pd/AC catalyst.

Entry	Catalyst	Reaction Temperature (°C)	Conversion of Dipentene (%)	Selectivity of p-Cymene (%)	Content of p-Cymene (%)
1	10% Pd/AC (First run)	220	100	82.26	82.26
2	10% Pd/AC (Second run)	220	100	74.69	74.69
3	10% Pd/AC (Third run)	220	100	67.22	67.22
4	10% Pd/AC (Forth run)	220	95.39	60.99	63.94

To further investigate the stability of Pd/CTF and Pd/AC, the spent catalyst used three times in the conversion was collected and characterized by TEM and XPS techniques. As displayed in the TEM image, the primary morphology of 5% Pd/CTF was kept after the conversion (Figure S1d). After reactions, the Pd particles were still well dispersed on CTF support, and the size of the Pd particles increased from 2.82 nm to 6.03 nm. Pd particles agglomerated to some extent, even if the CTF may hinder this phenomenon by the interactions between nitrogen and palladium. In comparison, the size of the palladium particles increased from 3.81 nm to 7.47 nm for Pd/AC (Figure S1e,f). The aggregation degree of Pd/AC is stronger than that of Pd/CTF. This is precisely because of the phenomenon of Pd nanoparticle agglomeration caused by 10% Pd/AC without nitrogen sites [54].

It is reasonable that the rich nitrogen in CTF enhances the interaction between Pd and CTF, and is responsible for the superior recyclability in the dehydrogenation of dipentene.

All the above experimental studies fully proved that Pd/CTF catalysts had good catalytic effects and stability in catalyzing the dehydrogenation of dipentene for the preparation of p-cymene.

3. Materials and Methods

3.1. Materials

Sodium hydroxide (NaOH, 96.0%), concentrated hydrochloric acid (HCl, AR), and borohydride ($NaBH_4$, 96%) were purchased from the China Sinopharm Chemical Reagent Co. Ltd. Dipentene ($C_{10}H_{16}$, 95%), potassium chloride (KCl, 99%), lithium chloride (LiCl, 98%), zinc chloride ($ZnCl_2$, 98%), and terephthalonitrile ($C_8H_4N_2$, 98%) were obtained from Shanghai Aladdin Biochemical Technology Co., Ltd. (Shanghai, China).

Palladium on activated carbon (10% Pd, 50% wet with water for safety) and palladium chloride ($PdCl_2$, 99%) were purchased from Shanghai Bide Pharmaceutical Technology Co., Ltd. (Shanghai, China).

Raney Ni was purchased from Shanghai Rhawn Chemical Reagent Co., Ltd. (Shanghai, China). Argon (99.999%) and nitrogen (99.99%) gases were provided by Fujian Nanan Chenggong Gas Co. Ltd. (Fujian, China).

Ultra-pure water (18 mW cm^{-1}) was acquired from water purification equipment (Millipore, Milli-Q, Darmstadt, Germany). All reagents were commercially available and used without further purification. The industrial dipentene was obtained from Fujian Nanping Qingsong Chemical Co., Ltd. (Fujian, China).

3.2. Synthesis of Catalysts

3.2.1. Synthesis of CTF

Terephthalonitrile (1 g, 7.80 mmol), sodium chloride (0.11 g, 1.88 mmol), potassium chloride (0.14 g, 1.88 mmol), and zinc chloride (0.75 g, 5.50 mmol) were uniformly mixed with a quartz mortar (50 mL) to obtain a mixed powder. The mixed powders were calcined in a tube furnace at an elevated temperature rate of 2 °C/min to 300 °C under nitrogen for 6 h and then cooled naturally to room temperature. The solids were grounded into a powder and added to 300 mL of water. The suspension was stirred at 80 °C for 12 h, and then collected by suction filtration. Then, the solid was redispersed in a 300 mL hydrochloric acid solution with a concentration of 1.0 mol/L and stirred for 12 h, and then washed with water eight times to neutral. Then the solid was purified by Soxhlet extraction with methanol as a solvent at 95 °C for 24 h, followed by Soxhlet extraction with dichloromethane at 70 °C for 24 h, and then dried in a vacuum oven at 70 °C for 12 h to obtain a yellow powder of CTF material.

3.2.2. Synthesis of x% Pd/CTF

0.15 g of CTF was added with the typical amount of $PdCl_2$ and 2 mL of 2 mol/L hydrochloric acid (HCl mass concentration: 0.73 wt%) and 18 mL of water. After ultrasonically assisted dispersion for 30 min, the mixture was stirred and heated to reflux at 80 °C for 8 h. Then the solution was cooled to room temperature, and then 1 mol/L NaOH solution was added to adjust the pH to 10, and then slowly dropwise added with 1.1 mL 0.1 mol/L $NaBH_4$ solution. Subsequently, the reaction was stirred for 2 h at room temperature and then separated by filtration. The resultant precipitate was washed with water until the filtrate was neutral, dried in a vacuum at 60 °C, and then dried at 60 °C for 12 h in a vacuum. The as-obtained sample is Pd loaded covalent triazine frameworks (denoted as x% Pd/CTF), in which x represents the theoretical weight percentage of Pd relative to CTF material.

3.3. Measurements and Instruments

Scanning electron microscopy (SEM, Hitachi Co., Tokyo, Japan, Hitachi S-4800) was used to examine the morphology of the synthesized catalysts. Transmission electron microscopy (TEM, ThermoFisher Scientific, Waltham, MA, USA, Talos F200X G2) was used for morphological observation of the prepared samples, and chemical compositions of catalytic materials were analyzed using energy dispersive spectrometers (EDS). To investigate the crystal structure of catalysts, X-ray powder diffraction analysis was carried out using an X-ray diffractometer (Rigaku Co., Tokyo, Japan, Smart lab) equipped with a Cu Kα (λ = 1.5418 Å) radiation source. For determining functional groups and chemical structures of the catalyst, Fourier transform infrared spectrophotometer (FT-IR, Nicolet, Madison, WI, USA, Nicolet iS10) was used. XPS measurements were made using an instrument (ThermoFisher Scientific, Waltham, MA, USA, K-Alpha$^+$) with a monochromatized Al Kα line source (200 W). In all binding energies, the C 1s peak at 284.8 eV of surface adventitious carbon was used as a reference.

3.4. Catalytic Dehydrogenation of Industrial Dipentene

The catalytic dehydrogenation of industrial dipentene was performed in a stainless-steel autoclave (CEL-HPR100T$^+$, Ceaulight, Beijing, China) equipped with a 100 mL of

inner quartz reaction bottle. Under 0.1 MPa of Ar gas, 5 g of industrial dipentene and 0.1 g of catalyst were added to a quartz liner with a stirring rate of 300 rpm and heated at the temperature of 220 °C for 2 h. The obtained solid was separated after the reaction by centrifugation. For different catalytic tests, the same amount of catalyst ($0.1\times$ *g*) is used.

The liquid products were collected and diluted with ethanol for further analysis. The amounts of industrial dipentene and p-cymene were analyzed by Intuvo 9000 gas chromatography-mass spectrometry (GC-MS) (Agilent Co., Santa Clara, CA, USA) with a HP-5MS UI column (30 m × 0.25 mm × 0.25 μm, Agilent, Santa Clara, CA, USA) in a multiple reaction monitoring (MRM) mode.

Helium was used as a carrier gas at a flow rate of 0.8 mL min^{-1}. An oven temperature program was set from 56 °C, to 83 °C at 3° min^{-1}, held for 1 min; to 89 °C at 1° min^{-1}, held for 2 min; and to 94 °C at 0.5° min^{-1}, held for 1 min; to 110 °C at 4° min^{-1}, held for 0 min. With a split flow rate of 16 mL min^{-1}, and an injection ratio of 20, the sample was injected with 250 °C in the injector and detector.

The conversion rate of dipentene to dehydrogenation products and the selectivity of cymene were calculated according to Formulas (1) and (2), respectively.

$$\text{Conversion rate of dipentene}/\% = (M_{D1} - M_{D2})/M_{D1} \times 100 \quad (1)$$

$$\text{Selectivity of p-cymene}/\% = M_O/(M_{D1} - M_{D2}) \times 100 \quad (2)$$

There are three mass fractions represented in the formula: M_{D1} for dipentene in the raw material; M_{D2} for dipentene in the reaction product; and M_O for p-cymene in the reaction product.

4. Conclusions

Palladium loaded covalent triazine frameworks nanocomposites (Pd/CTF) were prepared by molten-salt approach and chemical reduction methods. Pd/CTF was designed as an effective catalyst for the catalytic dehydrogenation of industrial dipentene to p-cymene. In comparison with commercial Pd/AC, Pd/CTF with Pd loading mass amount of 5% showed the highest efficiency in the dehydrogenation of dipentene to p-cymene with a high conversion rate of 100% and selectivity for p-cymene of 96%, and also maintained high stability during the recycling test. The strong interaction between Pd nanoparticles and CTF and the enhanced electron transfer at the metal-semiconductor interface contribute to the remarkable catalytic activity for dehydrogenation of dipentene to p-cymene. This work opens up new opportunities for the development of highly efficient catalysts for biomass conversion into high-value-added chemical products.

Supplementary Materials: The following supporting information can be downloaded at: https://www.mdpi.com/article/10.3390/catal13091248/s1, Figure S1: TEM images and corresponding size distribution curves of Pd nanoparticles for (a) 1% Pd/CTF, (b) 3% Pd/CTF, (c) 7% Pd/CTF, (d) 5% Pd/CTF-reused, (e) 10% Pd/AC, and (f) 10% Pd/AC-reused samples; Figure S2: XPS spectra of (a) survey, (b) Pd 3d, (c) C 1s, and (d) N 1s for CTF and Pd/CTF catalysts with different Pd loading contents; Figure S3: XPS spectra of Pd 3d for (a) 5% Pd/CTF and (b) 10% Pd/AC catalyst before and after dehydrogenation reactions; Figure S4: XPS spectra of (a) C 1s, and (b) N 1s for 5% Pd/CTF catalyst before and after dehydrogenation reactions; Table S1: Pd particle sizes, Pd^0 ratios and Pd^{2+} ratios of Pd/CTF and Pd/AC catalysts; Table S2: XPS fitting results of CTF and Pd/CTF catalysts with different Pd loading contents.

Author Contributions: Data curation, Y.L., Y.C. (Yonghui Chen) and Y.W.; Investigation, Z.X.; Funding acquisition, X.R., Y.Z. and Y.C. (Yilin Chen); Project administration, X.R.; Supervision, X.R., Y.C. (Yilin Chen) and Y.Z.; Writing—original draft, Y.C. (Yonghui Chen) and Y.Z.; Writing—review and editing, Y.C. (Yilin Chen) and J.J. All authors have read and agreed to the published version of the manuscript.

Funding: This research was funded by the Scientific and Technological Projects of Nanping (N2020Z015), the Natural Science Foundation of Fujian Province (2023J01115 and 2023J01117), the National Natural Science Foundation of China (21902051), the Fundamental Research Funds for the Central Universities (ZQN-807) and the Open Research Fund of Academy of Advanced Carbon Conversion Technology, Huaqiao University (AACCT0005).

Data Availability Statement: Not applicable.

Acknowledgments: The authors thank Qiuxiang Wang and Junyu Zhang from Instrumental Analysis Center of Huaqiao University for XPS and TEM analysis. The authors thank Xiaohong Yuan from Xiamen Institute of Rare Earth Materials, Haixi Institute, Chinese Academy of Sciences for GC-MS analysis.

Conflicts of Interest: The authors declare no conflict of interest.

References

1. Weyrich, P.A.; Hölderich, W.; van Daelen, M.A.; Gorman, A.M. Theoretical and experimental study on the selectivity of dehydrogenation of α-limonene in ZSM-5 and zeolite-Y. *Catal. Lett.* **1998**, *52*, 7–12. [CrossRef]
2. Grau, R.J.; Zgolicz, P.D.; Gutierrez, C.; Taher, H.A. Liquid phase hydrogenation, isomerization and dehydrogenation of limonene and derivatives with supported palladium catalysts. *J. Mol. Catal. A Chem.* **1999**, *148*, 203–214. [CrossRef]
3. Cattaneo, S.; Stucchi, M.; Villa, A.; Prati, L. Gold Catalysts for the Selective Oxidation of Biomass-Derived Products. *ChemCatChem* **2019**, *11*, 309–323. [CrossRef]
4. Ozturk, B.; Winterburn, J.; Gonzalez-Miquel, M. Orange peel waste valorisation through limonene extraction using bio-based solvents. *Biochem. Eng. J.* **2019**, *151*, 107298. [CrossRef]
5. Zhang, Q.-G.; Bi, L.-W.; Zhao, Z.-D.; Chen, Y.-P.; Li, D.-M.; Gu, Y.; Wang, J.; Chen, Y.-X.; Bo, C.-Y.; Liu, X.-Z. Application of ultrasonic spraying in preparation of p-cymene by industrial dipentene dehydrogenation. *Chem. Eng. J.* **2010**, *159*, 190–194. [CrossRef]
6. Catrinescu, C.; Fernandes, C.; Castilho, P.; Breen, C. Influence of exchange cations on the catalytic conversion of limonene over Serra de Dentro (SD) and SAz-1 clays - Correlations between acidity and catalytic activity/selectivity. *Appl. Catal. A Gen.* **2006**, *311*, 172–184. [CrossRef]
7. Fernandes, C.; Catrinescu, C.; Castilho, P.; Russo, P.A.; Carrott, M.R.; Breen, C. Catalytic conversion of limonene over acid activated Serra de Dentro (SD) bentonite. *Appl. Catal. A Gen.* **2007**, *318*, 108–120. [CrossRef]
8. Marchese, A.; Arciola, C.R.; Barbieri, R.; Silva, A.S.; Nabavi, S.F.; Tsetegho Sokeng, A.J.; Izadi, M.; Jafari, N.J.; Suntar, I.; Daglia, M.; et al. Update on Monoterpenes as Antimicrobial Agents: A Particular Focus on p-Cymene. *Materials* **2017**, *10*, 947. [CrossRef] [PubMed]
9. Tibbetts, J.D.; Russo, D.; Lapkin, A.A.; Bull, S.D. Efficient Syntheses of Biobased Terephthalic Acid, p-Toluic Acid, and p-Methylacetophenone via One-Pot Catalytic Aerobic Oxidation of Monoterpene Derived Bio-p-cymene. *ACS Sustain. Chem. Eng.* **2021**, *9*, 8642–8652. [CrossRef] [PubMed]
10. Clark, J.H.; Macquarrie, D.J.; Sherwood, J. A quantitative comparison between conventional and bio-derived solvents from citrus waste in esterification and amidation kinetic studies. *Green Chem.* **2012**, *14*, 90–93. [CrossRef]
11. Ye, L.; Thompson, B.C. p-Cymene: A Sustainable Solvent that is Highly Compatible with Direct Arylation Polymerization (DArP). *ACS Macro Lett.* **2021**, *10*, 714–719. [CrossRef]
12. Granato, A.V.; Santos, A.G.; dos Santos, E.N. p-Cymene as Solvent for Olefin Metathesis: Matching Efficiency and Sustainability. *ChemSusChem* **2017**, *10*, 1832–1837. [CrossRef]
13. Roberge, D.M.; Buhl, D.; Niederer, J.P.M.; Hölderich, W.F. Catalytic aspects in the transformation of pinenes to p-cymene. *Appl. Catal. A Gen.* **2001**, *215*, 111–124. [CrossRef]
14. Martin-Luengo, M.A.; Yates, M.; Rojo, E.S.; Huerta Arribas, D.; Aguilar, D.; Ruiz Hitzky, E. Sustainable p-cymene and hydrogen from limonene. *Appl. Catal. A Gen.* **2010**, *387*, 141–146. [CrossRef]
15. Tavera Ruiz, C.P.; Gauthier-Maradei, P.; Capron, M.; Pirez, C.; Gardoll, O.; Katryniok, B.; Dumeignil, F. Transformation of dl Limonene into Aromatic Compounds Using Supported Heteropolyacid Catalysts. *Catal. Lett.* **2019**, *149*, 328–337. [CrossRef]
16. Satira, A.; Espro, C.; Paone, E.; Calabro, P.S.; Pagliaro, M.; Ciriminna, R.; Mauriello, F. The Limonene Biorefinery: From Extractive Technologies to Its Catalytic Upgrading into p-Cymene. *Catalysts* **2021**, *11*, 387. [CrossRef]
17. Makarouni, D.; Lycourghiotis, S.; Kordouli, E.; Bourikas, K.; Kordulis, C.; Dourtoglou, V. Transformation of limonene into p-cymene over acid activated natural mordenite utilizing atmospheric oxygen as a green oxidant: A novel mechanism. *Appl. Catal. B Environ.* **2018**, *224*, 740–750. [CrossRef]
18. Rachwalik, R.; Hunger, M.; Sulikowski, B. Transformations of monoterpene hydrocarbons on ferrierite type zeolites. *Appl. Catal. A Gen.* **2012**, *427–428*, 98–105. [CrossRef]
19. Lycourghiotis, S.; Makarouni, D.; Kordouli, E.; Bourikas, K.; Kordulis, C.; Dourtoglou, V. Activation of natural mordenite by various acids: Characterization and evaluation in the transformation of limonene into p-cymene. *Mol. Catal.* **2018**, *450*, 95–103. [CrossRef]

20. Retajczyk, M.; Wroblewska, A. The Isomerization of Limonene over the Ti-SBA-15 Catalyst-The Influence of Reaction Time, Temperature, and Catalyst Content. *Catalysts* **2017**, *7*, 273. [CrossRef]
21. Retajczyk, M.; Wróblewska, A. Isomerization and Dehydroaromatization of R(+)-Limonene Over the Ti-MCM-41 Catalyst: Effect of Temperature, Reaction Time and Catalyst Content on Product Yield. *Catalysts* **2019**, *9*, 508. [CrossRef]
22. Cui, H.; Zhang, J.; Luo, Z.; Zhao, C. Mechanisms into dehydroaromatization of bio-derived limonene to p-cymene over Pd/HZSM-5 in the presence and absence of H_2. *RSC Adv.* **2016**, *6*, 66695–66704. [CrossRef]
23. Yılmazoğlu, E.; Akgün, M. p-Cymene production from orange peel oil using some metal catalyst in supercritical alcohols. *J. Supercrit. Fluids* **2018**, *131*, 37–46. [CrossRef]
24. Du, J.M.; Xu, H.L.; Shen, J.; Huang, J.J.; Shen, W.; Zhao, D.Y. Catalytic dehydrogenation and cracking of industrial dipentene over M/SBA-15 (M=A1, Zn) catalysts. *Appl. Catal. A Gen.* **2005**, *296*, 186–193. [CrossRef]
25. Kamitsou, M.; Panagiotou, G.D.; Triantafyllidis, K.S.; Bourikas, K.; Lycourghiotis, A.; Kordulis, C. Transformation of α-limonene into p-cymene over oxide catalysts: A green chemistry approach. *Appl. Catal. A Gen.* **2014**, *474*, 224–229. [CrossRef]
26. Buhl, D.; Roberge, D.M.; Holderich, W.F. Production of p-cymene from α-limonene over silica supported Pd catalysts. *Appl. Catal. A Gen.* **1999**, *188*, 287–299. [CrossRef]
27. Alsharif, A.; Smith, N.; Kozhevnikova, E.F.; Kozhevnikov, I.V. Dehydroisomerisation of α-Pinene and Limonene to p-Cymene over Silica-Supported ZnO in the Gas Phase. *Catalysts* **2021**, *11*, 1245. [CrossRef]
28. Alsharif, A.; Kozhevnikova, E.F.; Kozhevnikov, I.V. Selective dehydroisomerization of cyclic monoterpenes to p-cymene over silica-supported CdO. *Appl. Catal. B Environ.* **2023**, *325*, 122362. [CrossRef]
29. Weyrich, P.A.; Hölderich, W.F. Dehydrogenation of α-limonene over Ce promoted, zeolite supported Pd catalysts. *Appl. Catal. A Gen.* **1997**, *158*, 145–162. [CrossRef]
30. Zheng, Y.; Chen, Y.; Wang, L.; Tan, M.; Xiao, Y.; Gao, B.; Lin, B. Metal-free 2D/2D heterostructured photocatalyst of black phosphorus/covalent triazine-based frameworks for water splitting and pollutant degradation. *Sustain. Energy Fuels* **2020**, *4*, 3739–3746. [CrossRef]
31. Li, L.; Fang, W.; Zhang, P.; Bi, J.; He, Y.; Wang, J.; Su, W. Sulfur-doped covalent triazine-based frameworks for enhanced photocatalytic hydrogen evolution from water under visible light. *J. Mater. Chem. A* **2016**, *4*, 12402–12406. [CrossRef]
32. Wang, J.; Yu, Y.; Yu, H.; Wang, W.; Shen, L.-L.; Zhang, G.-R.; Mei, D. Covalent Triazine Framework Encapsulated Ultrafine PdAu Alloy Nanoclusters as Additive-Free Catalysts for Efficient Hydrogen Production from Formic Acid. *ACS Catal.* **2023**, *13*, 5135–5146. [CrossRef]
33. Li, W.-J.; Chen, Y.-X.; Kang, S.-L.; Mo, L.-P.; Zhang, Z.-H. Design, Synthesis and Characterization of Palladium-Functionalized Covalent Organic Framework and Its Application as Heterogeneous Catalysis for C-H Arylation of Azoles. *Chemistry* **2023**, *29*, e202301310. [CrossRef]
34. Chen, X.; Luo, L.; Zhang, Y.; Zhao, X. Theoretical Screening of Highly Efficient Single-Atom Catalysts Based on Covalent Triazine Frameworks for Oxygen Reduction. *Langmuir* **2023**, *39*, 6905–6913. [CrossRef]
35. Zhang, L.; Yu, H.; Wu, W.; Ge, Q.; Ni, S.; Song, C.; Huang, K. Ultrafine Palladium Embedded in N-doped Porous Carbon Material from Carbazole-covalent Triazine Polymer for Green Suzuki-Miyaura Coupling Reaction. *Chemnanomat* **2022**, *8*, e202200215. [CrossRef]
36. Wang, J.; Yu, Y.; Xu, W.; Yu, H.; Zhang, W.; Huang, H.; Zhang, G.-R.; Mei, D. Covalent triazine framework encapsulated Pd nanoclusters for efficient hydrogen production via ammonia borane hydrolysis. *J. Catal.* **2022**, *411*, 72–83. [CrossRef]
37. Wang, X.; Maeda, K.; Thomas, A.; Takanabe, K.; Xin, G.; Carlsson, J.M.; Domen, K.; Antonietti, M. A metal-free polymeric photocatalyst for hydrogen production from water under visible light. *Nat. Mater.* **2009**, *8*, 76–80. [CrossRef]
38. Li, Z.; Di, M.; Zhang, Y.; Zhang, B.; Zhang, Z.; Zhang, Z.; Li, A.; Qiao, S. Covalent Triazine Frameworks with Palladium Nanoclusters as Highly Efficient Heterogeneous Catalysts for Styrene Oxidation. *ACS Appl. Polym. Mater.* **2022**, *4*, 1047–1054. [CrossRef]
39. Bi, J.; Fang, W.; Li, L.; Wang, J.; Liang, S.; He, Y.; Liu, M.; Wu, L. Covalent Triazine-Based Frameworks as Visible Light Photocatalysts for the Splitting of Water. *Macromol. Rapid Comm.* **2015**, *36*, 1799–1805. [CrossRef]
40. Lan, Z.-A.; Wu, M.; Fang, Z.; Zhang, Y.; Chen, X.; Zhang, G.; Wang, X. Ionothermal Synthesis of Covalent Triazine Frameworks in a NaCl-KCl-ZnCl2 Eutectic Salt for the Hydrogen Evolution Reaction. *Angew. Chem. Int. Ed.* **2022**, *61*, e202201482. [CrossRef]
41. Huang, J.; Cui, W.-R.; Wang, Y.-G.; Yan, R.-H.; Jiang, W.; Zhang, L.; Liang, R.-P.; Qiu, J.-D. Rational designed molecularly imprinted triazine-based porous aromatic frameworks for enhanced palladium capture via three synergistic mechanisms. *Chem. Eng. J.* **2022**, *430*, 132962. [CrossRef]
42. Lu, Y.; He, J.; Chen, Y.; Wang, H.; Zhao, Y.; Han, Y.; Ding, Y. Effective Acetylene/Ethylene Separation at Ambient Conditions by a Pigment-Based Covalent-Triazine Framework. *Macromol. Rapid Comm.* **2018**, *39*, 1700468. [CrossRef] [PubMed]
43. Bulushev, D.A.; Golub, F.S.; Trubina, S.V.; Zvereva, V.V.; Bulusheva, L.G.; Gerasimov, E.Y.; Navlani-Garcia, M.; Krot, A.D.; Jena, H.S. Single-Atom Pd Catalysts Supported on Covalent Triazine Frameworks for Hydrogen Production from Formic Acid. *ACS Appl. Nano Mater.* **2022**, *5*, 12887–12896. [CrossRef]
44. Li, J.; Zhang, L.; Liu, X.; Shang, N.; Gao, S.; Feng, C.; Wang, C.; Wang, Z. Pd nanoparticles supported on a covalent triazine-based framework material: An efficient and highly chemoselective catalyst for the reduction of nitroarenes. *New J. Chem.* **2018**, *42*, 9684–9689. [CrossRef]

45. Raza, A.A.; Ravi, S.; Tajudeen, S.S.; Sheriff, A.K.I. Sulfonated covalent triazine polymer loaded with Pd nanoparticles as a bifunctional catalyst for one pot hydrogenation esterification reaction. *J. Solid State Chem.* **2021**, *302*, 122417. [CrossRef]
46. Guo, S.; Xiao, Y.; Jiang, B. Encapsulation of Pd Nanoparticles in Covalent Triazine Frameworks for Enhanced Photocatalytic CO2 Conversion. *ACS Sustain. Chem. Eng.* **2021**, *9*, 12646–12654. [CrossRef]
47. Chen, Y.-J.; Zhuo, H.-Y.; Pan, Y.; Liang, J.-X.; Liu, C.-G.; Li, J. Triazine COF-supported single-atom catalyst (Pd-1/trzn-COF) for CO oxidation. *Sci. China Mater.* **2021**, *64*, 1939–1951. [CrossRef]
48. He, T.; Liu, L.; Wu, G.; Chen, P. Covalent triazine framework-supported palladium nanoparticles for catalytic hydrogenation of N-heterocycles. *J. Mater. Chem. A* **2015**, *3*, 16235–16241. [CrossRef]
49. Zhao, L.; Shi, S.; Zhu, G.; Liu, M.; Gao, J.; Xu, J. Au-Pd alloy cooperates with covalent triazine frameworks for the catalytic oxidative cleavage of beta-O-4 linkages. *Green Chem.* **2019**, *21*, 6707–6716. [CrossRef]
50. Ding, S.-Y.; Wang, P.-L.; Yin, G.-L.; Zhang, X.; Lu, G. Energy transfer in covalent organic frameworks for visible-light-induced hydrogen evolution. *Int. J. Hydrogen Energ.* **2019**, *44*, 11872–11876. [CrossRef]
51. Zhu, H.; Wang, W.D.; Li, F.; Sun, X.; Li, B.; Song, Q.; Kou, J.; Ma, K.; Ren, X.; Dong, Z. Facile preparation of ultrafine Pd nanoparticles anchored on covalent triazine frameworks catalysts for efficient N-alkylation. *J. Colloid Interface Sci.* **2022**, *606*, 1340–1351. [CrossRef]
52. Guo, P.; Zhan, Y.; Yang, Y.; Lu, T. Preparation of COFs Supported Pd as an Efficient Catalyst for the Hydrogenation of Aromatic Nitro. *Catal. Lett.* **2022**, *152*, 3725–3732. [CrossRef]
53. Li, J.H.; Yu, Z.W.; Gao, Z.; Li, J.Q.; Tao, Y.; Xiao, Y.X.; Yin, W.H.; Fan, Y.L.; Jiang, C.; Sun, L.J.; et al. Ultralow-Content Palladium Dispersed in Covalent Organic Framework for Highly Efficient and Selective Semihydrogenation of Alkynes. *Inorg. Chem.* **2019**, *58*, 10829–10836. [CrossRef] [PubMed]
54. Ma, H.-C.; Kan, J.-L.; Chen, G.-J.; Chen, C.-X.; Dong, Y.-B. Pd NPs-Loaded Homochiral Covalent Organic Framework for Heterogeneous Asymmetric Catalysis. *Chem. Mater.* **2017**, *29*, 6518–6524. [CrossRef]

Disclaimer/Publisher's Note: The statements, opinions and data contained in all publications are solely those of the individual author(s) and contributor(s) and not of MDPI and/or the editor(s). MDPI and/or the editor(s) disclaim responsibility for any injury to people or property resulting from any ideas, methods, instructions or products referred to in the content.